

Article

Cyclic Lateral Loading Behavior of Thin-Shell Precast Concrete Wall Panels

Tugce Sevil Yaman ^{1,*}  and Gregory Lucier ² ¹ Civil Engineering Department, Mersin University, 33343 Mersin, Turkey² Department of Civil, Construction, and Environmental Engineering, North Carolina State University, Raleigh, NC 27695, USA; gwlucaier@ncsu.edu

* Correspondence: tsevilyaman@mersin.edu.tr; Tel.: +90-324-361-00-01

Abstract: Two precast concrete thin-shell wall panels were subjected to reverse-cyclic lateral loads to replicate wind fatigue over a 50-year design lifetime prior to loading to failure. The panels consisted of an outer wythe of concrete connected to light-gauge steel framing. Wire mesh was used to reinforce the concrete panel skin. Rivets provided a connection between the steel studs and the concrete panel. Two reinforced concrete (R/C) beams were integrated into the top and bottom parts of the panel, isolated from the concrete face by a thin sheet of extruded polystyrene (XPS) foam insulation. To connect these beams with the concrete face through the rigid foam insulation, a carbon-fiber-reinforced polymer (CFRP) grid was utilized. The aim of the experimental program was to characterize the behavior of the concrete and steel framing panel, with particular attention focused on the connections between the various structural elements of the panel. The first and second thin-shell panels survived the fatigue loading cycles and behaved elastically through failure-level lateral load cycles equivalent to 54 psf (2.6 kPa) and 66 psf (3.2 kPa) of applied uniform load, respectively. The failure mode was the separation of the top R/C beam from the concrete panel on the pull stroke of the loading cycle (when the connection between the beam and the concrete shell was in tension) for both specimens.

Keywords: precast thin-shell wall panel; concrete panel; steel stud; CFRP grid; wire mesh; rivets



Citation: Sevil Yaman, T.; Lucier, G. Cyclic Lateral Loading Behavior of Thin-Shell Precast Concrete Wall Panels. *Buildings* **2023**, *13*, 2750. <https://doi.org/10.3390/buildings13112750>

Academic Editor: Rajai Zuheir Al-Rousan

Received: 30 August 2023

Revised: 21 October 2023

Accepted: 30 October 2023

Published: 31 October 2023



Copyright: © 2023 by the authors. Licensee MDPI, Basel, Switzerland. This article is an open access article distributed under the terms and conditions of the Creative Commons Attribution (CC BY) license (<https://creativecommons.org/licenses/by/4.0/>).

1. Introduction

Lightweight precast concrete wall systems can integrate a thin outer wythe of concrete, typically varying between 1.5 in. (38 mm) and 3 in. (76 mm) in thickness, with a back-up system usually constructed of light cold-formed steel framing. These systems are commonly referred to as thin-shell wall panels or stud–concrete panels, with the combination of these two materials providing a “skin and bones” wall structure. These types of panels can be designed as structural or non-structural walls. In the structural (i.e., load-bearing) condition, panels are often required to support vertical loads from the roof. In either condition, panels must carry the out-of-plane forces created by wind pressure and suction acting on the skin of the building. The thin shell of concrete also resists in-plane loads and braces the steel studs, while the steel framing is designed to carry axial loads and works with the concrete shell to resist the bending created by out-of-plane forces. Thermally isolating the exterior concrete shell from the interior structure is an important consideration for the energy efficiency of the finished structure, so connectors are used to join the concrete shell and the steel studs across a small air gap. Welded wire reinforcement is used to reinforce the concrete shell. Structural concrete beams integrated into the panel’s top and bottom edges are also gapped from the concrete shell for thermal efficiency by a thin layer of foam insulation. Structural connectors cross this joint, and the integrated concrete beams are attached to the steel studs at the top and bottom through a light-gauge steel track.

The system provides a finished structure with a traditional wall cavity for utilities and allows for installing interior finished surfaces without furring strips (i.e., the studs are

accessible on the inner surface of the wall for attachment of drywall or similar). Such wall panels can be produced in many different sizes, limited only by transportation and handling restrictions. The height of a typical panel usually corresponds with the story height of the structure, often from 8 ft. (2.4 m) to more than 12 ft. (3.7 m), and the panel length can be up to 30 ft. (9.1 m) or more, as required by the specific project. Stud–concrete panels can be designed to bear gravity loads, withstand lateral wind or seismic loads in or out of plane, provide insulation, and supply finished exterior wall surfaces. Thin-shell systems lessen the weight of the wall structure compared with other precast wall systems and provide advantages, including reduced dead loads, accelerated construction schedules, thermal efficiency and durability for sustainable construction, and improved climate control inside the finished structure due to effects from thermal mass.

The integrated concrete beams at the ends of the panel act to spread out concentrated loads from a potential roof system or simply from the weight of the panel. The beams also provide a convenient and sturdy connection point to attach the panels to each other and to the horizontal diaphragms at the floor and roof levels. The beams also provide handling points during production and construction. In order to achieve greater thermal efficiency by preventing thermal bridges, a carbon-fiber-reinforced polymer (CFRP) grid with very low thermal conductivity was used to connect the integrated concrete beams to the thin concrete face shell across a thin layer of rigid polystyrene insulation.

2. Background

Even though there exist numerous studies about the performance of prestressed concrete sandwich panels having inner and outer faces of concrete separated by rigid insulation, there are very few studies concerning sandwich panels' long-term behavior under fatigue loading. In particular, very few studies at all of the thin-shell precast wall panels are found in the literature. Of course, plenty of studies exist on lightweight steel structural systems with various skins that are not precast concrete. Several researchers have investigated the usage of fiber-reinforced polymer (FRP) shear connectors for improving structural performance and preventing thermal bridges. The status of the area is outlined below.

Rubio et al. [1] developed an innovative lightweight ceramic precast composite panel system, one of the few published examples of thin-shell precast systems. The panel was economical and of high performance, touting efficient manufacturing techniques and enhanced thermal performance over traditional systems. The applicability of the system was proved by experiments and by multiple successful case studies. An experimental program was carried out on the ceramic precast composite panels, including flexural, racking shear, and concentrated load tests on modest-scale specimens (roughly 4 ft. × 8 ft. or 1.2 m × 2.4 m). Moreover, fire resistance, hose stream resistance, and thermal efficiency experiments were also performed. The panel system demonstrated suitable structural behavior, thermal and energy efficiency, lightness, and fire performance.

Hofheins et al. [2] conducted experiments on precast concrete panels to examine the behavior of loose-plate connectors under cyclic loading. It was observed that the connection showed low ductility. Pessiki and Mlynarczyk [3] studied the behavior of sandwich panels under lateral loading and examined the contribution of solid concrete areas, mechanical wythe connecting elements, and bond to composite action. It was observed that the concrete solid regions provided the best stiffness and strength, thus contributing most to the composite behavior but with the worst thermal performance. Choi et al. [4] evaluated the insulated concrete sandwich panels' composite action having GFRP shear grids under monotonic loading and cyclic loading, simulating wind pressure and suction. The levels of composite behavior regarding initial stiffness, shear flow, and ultimate strength were compared. In addition, the fatigue effect was analyzed. Results showed that XPS foam contributed substantially to the composite behavior. Better composite behavior was observed for the monotonic loading case than for the cyclic loading case. Also, fatigue tests on partially composite precast insulated concrete sandwich panels with either steel or basalt

FRP reinforcement and shear connecting elements were carried out by Teixeira and Fam [5] under cyclic bending.

Sharafi et al. [6] summarized studies focused on lightweight steel frame (LSF) lateral loading capacity, especially those produced from thin gauge cold-formed steel (CFS). The review contained developments in shear walls covered with face sheathings, LSF-straped walls, custom bolted moment frames, podium structures, and hybrid structures. Researchers have performed a wide spectrum of studies to investigate the performances of various types of CFS systems. Tafti and Behnamfar [7] searched the influence of the number of studs at the end of the panels on the behavior of CFS shear panel bracings under cyclic load, simulating earthquake loading. In addition, Iuorio et al. [8] completed tests on the seismic behavior of CFS strap-braced panels, and they verified hypotheses for the design of these systems according to earthquake loads. Further, Accorti et al. [9], Liu et al. [10], Xu et al. [11], Lee et al. [12], Zhang et al. [13], and Belal et al. [14] carried out studies to investigate the CFS shear wall behavior under the reversed cyclic lateral load case.

Bao et al. [15] conducted an experimental program to explore a steel stud wall's lateral resistance when connected to a partly rigid steel frame. Tested parameters included section dimensions, stud spacing, and stud configuration and spacing. The behavior at failure, load-carrying capacity, energy dissipation, and stiffness of specimens were examined. It was seen that the stud system greatly enhanced the lateral load-carrying capacity and stiffness of the partly rigid frames. A wide range of research has been performed on different applications of lightweight steel frames tested under reversed-cyclic lateral load; however, none of the systems involved steel studs connected to a precast concrete shell. Prior studies include tests of light steel frames with wood panel sheathing as shear walls [16]; stud framed walls having strap bracing and steel covering [17]; steel stud framed walls utilized as braced bays [18]; steel frames with R/C infill walls [19]; non-structural lightweight steel drywall partitions [20]; concrete-filled steel tube truss shear walls [21]; steel-foam concrete composite panels [22]; steel-concrete tube shear walls having horizontal joints [23]; and shear panels formed of steel columns in concrete walls [24]. The research on composite shear panels showed that the ductility of the unmodified composite panel was lower than the reference panel ductility. Composite panels having gaps at the stud roots exhibited improved energy absorption and ductility [19].

3. Scope of the Research

The results of full-scale experiments on two precast non-load-bearing thin-shell wall panels, NLB-1 and NLB-2, where the abbreviation NLB indicates non-load-bearing, are presented in this paper. The panels were designed to support a uniform lateral wind loading that would result from a 120 mph (193 kmh) design wind speed. The loading sequence for the panels was developed to simulate wind fatigue over a 50-year design lifetime prior to loading to failure. Load and support conditions were designed to simulate design assumptions as closely as practical, with a pin connection at the bottom of the panel and a bi-directional slotted roller at the top (lateral motion restrained in both directions, but rotation and vertical motions were permitted). The aim of the testing program was to describe the performance of the two full-size precast thin-shell wall panels subjected to reverse-cyclic lateral loads. Related goals of particular interest included collecting data to characterize the behaviors of concrete panels and steel framing and to determine the degree of composite behavior that developed among the outer-wythe concrete, the concrete beams, and the steel studs at all levels of loading.

4. Experimental Program

4.1. Test Panels

The wall panels tested in the program consisted of a 12 ft. \times 14 ft. (3.7 m \times 4.3 m) outer shell of concrete that had a thickness of 2 in. (51 mm) and was attached to an 11.96 ft. \times 12 ft. (3.7 m \times 3.7 m) light-gauge steel stud frame of 6 in. (152 mm) depth. Wire mesh was utilized to reinforce the concrete shell. Two horizontal steel straps, one at a location of

4 ft. (1.2 m) from the steel framing’s bottom part and another 8 ft. (2.4 m) from the bottom, were used to space and brace the studs during assembly. Rivets connected to the steel stud flanges were cast into the concrete shell and supplied the connection between steel studs and concrete panel. Two integrated R/C beams, each with dimensions of 12 ft. × 1 ft. (3.7 m × 0.3 m) and thickness of 6 in. (152 mm), were included, one each at the top and bottom of each concrete panel. Rigid extruded polystyrene insulation 0.5 in. (13 mm) thick created a thermal break between the exterior concrete shell and the R/C beams. CFRP grid was utilized to connect the concrete shell and the beams across this insulation, thus transferring shear between the concrete components. Reverse-cyclic lateral loads simulating the effects of wind pressure and suction were applied during the tests, and no axial loading was applied. The elevation views of the concrete panel and the steel studs are demonstrated in Figures 1 and 2, respectively.

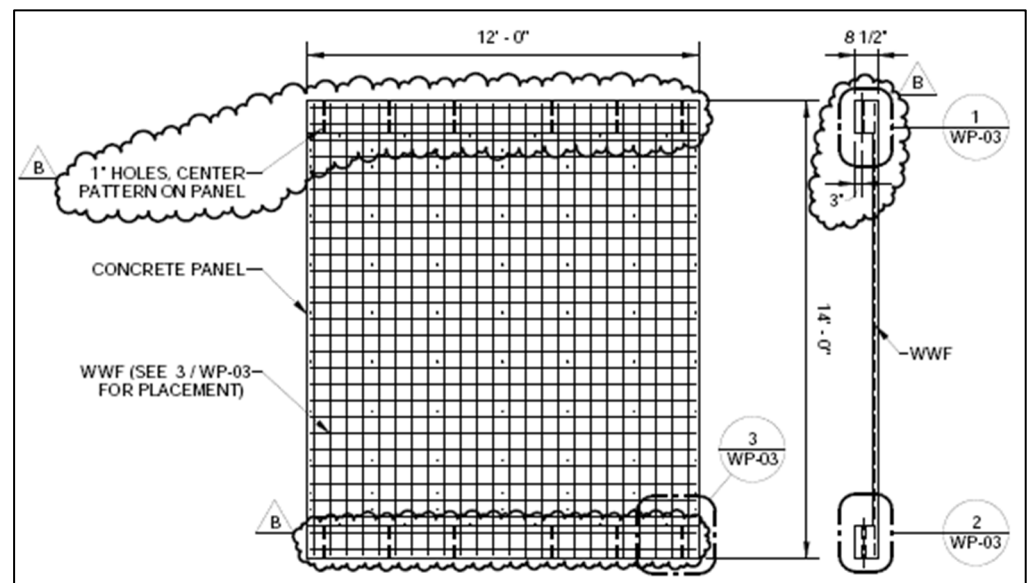


Figure 1. Elevation view of the concrete panel.

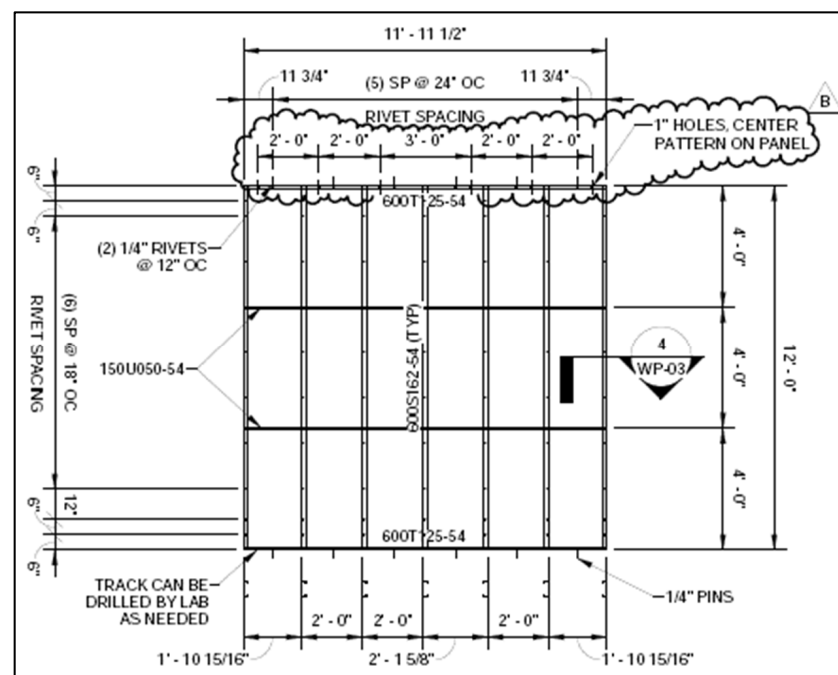


Figure 2. Elevation view of the steel stud frame.

4.2. Material Properties

The panels' mean concrete compressive strength at the time of testing was 8083 psi (56 MPa), as obtained from compressive testing of 4 in. × 8 in. (102 mm × 203 mm) concrete cylinders poured on the day of panel casting. The CFRP grid, cut at a 45° angle, is a lightweight, high-strength, and non-corrosive connector. It consists of carbon fiber tow impregnated with epoxy resin. The CFRP grid's mean strand tensile strength, as stated by the manufacturing company, is 290 ksi (2000 MPa).

The material characteristics of the XPS insulation are provided in Table 1.

Table 1. XPS insulation material [25].

Foam Type	Density [pcf]	Compressive Strength [psi]	Elastic Modulus [psi]
Extruded Polystyrene	1.55	25	675

Notes: 1 pcf = 157 N/m³, 1 psi = 6.9 kN/m², compressive strength listed at 10% deformation.

4.3. Construction of Wall Panels

The thin-shell wall panels were cast flat in steel production forms. Fabrication began by laying wire mesh reinforcement for the outer wythe of concrete. Then, the assembled steel frame with rivets protruding into the area where the concrete shell would be cast was placed. Steel framing consisted of vertical studs seated on a horizontal bottom steel track, called a sole plate, and capped with another steel track, called a top plate. Following the casting of a 2 in. (51 mm) thick concrete layer to form the outer concrete shell, XPS insulation and CFRP grids were placed at the concrete panel's top and bottom, above and below the steel tracks, with the CFRP grid pushed into the wet concrete beneath. With the CFRP grid protruding through the insulation, the top and bottom concrete beam reinforcement was placed, along with concrete for the beams. Embedded plates and hardware for connections and lifting devices were set in the fresh concrete.

4.4. Loading Sequence

The applied loading sequence consisted of several loading levels and approximately 4800 lateral load cycles in total per panel. The loading series is outlined in Table 2. A load cycle was defined as loading the specimen from unloaded state to a selected lateral load value in both directions. During the tests, equal lateral loads were applied at the quarter height and three-quarter height of each panel by hydraulic cylinders. These applied loads were selected and distributed on the panel to mimic the effects of a uniformly applied pressure.

The applied lateral loads corresponded to a service-level wind pressure of 60 psf (2.9 kPa). The lateral wind loading was calculated in accordance with the Minimum Design Loads for Buildings and Other Structures Standard (ASCE/SEI 7-16) [26] for a building classification II, an exposure category C, 200 ft. (61 m) building width, 250 ft. (76 m) building length, and a flat roof with 20 ft. (6.1 m) mean height. The topographic factor was taken as 1.0. Moreover, the factor of directionality was taken as 0.85 [2]. For the specified terms and 120 mph (193 kmh) design wind speed, the analytical method of ASCE/SEI 7-16 [26] predicted a 60 psf (2.9 kPa) wind pressure and a 60 psf (2.9 kPa) suction over the panel's face. The 60 psf (2.9 kPa) suction is equal to a total factorized concentrated lateral load of 10.08 kips (44.8 kN). This load was assumed to be the same magnitude in both directions for design so that loads of equal magnitude could be exerted in each direction of each cycle.

Table 2. Loading sequence.

Step Number	Applied Lateral Load Steps		
	Load Level [psf]	Load per Cylinder [kips]	Cycles Completed [#]
1	0	0	0
2	35% × 60 = 21 psf	1.75	4697
3	40% × 60 = 24 psf	2	96
4	45% × 60 = 27 psf	2.25	1
5	50% × 60 = 30 psf	2.5	1
6	60% × 60 = 36 psf	3	1
7	70% × 60 = 42 psf	3.5	1
8	80% × 60 = 48 psf	4	1
9	90% × 60 = 54 psf	4.5	1
10	100% × 60 = 60 psf	5	1
Continue to Failure	10% Increments		

Note: 1 psf = 0.048 kPa; 1 kips = 4.45 kN.

4.5. Reverse Cyclic Loading

It was desired to test each panel under fatigue loading to simulate the wind loading effect over the 50-year design lifetime. The Weibull distribution was used to rationally choose increments of loading and cycles in each increment, based on the works of Erich [27], Xu [28], and Manwell et al. [29].

The wind alteration for a characteristic location is defined utilizing the Weibull distribution to model the occurrence probability of specific wind speeds, where the PDF (probability distribution function) is stated by Equation (1) [29].

$$F(U) = 1 - \exp \left[- \left(\frac{U}{c} \right)^k \right] \quad (1)$$

In this case, $F(U)$ is the Weibull PDF, or probability distribution function. The parameter U is the wind speed being examined, and parameters k and c are the shape and scale factors, respectively.

The factors of shape and scale depend on the average wind speed and wind speeds' standard deviation. These factors can be calculated from wind data recorded in the field, and they change with respect to particular geographical position. If there is no field-recorded data, it is reasonable to take the value of shape factor as 2.0 [27,28]. Using this value, a specific configuration of the Weibull distribution named the Rayleigh distribution is obtained, where the ratio of the standard deviation to the average value is constant. Eventually, the Rayleigh distribution takes the form provided in Equation (2) [29], dependent just on the mean wind speed.

$$F(U) = 1 - \exp \left[- \frac{\pi}{4} \left(\frac{U}{\bar{U}} \right)^2 \right] \quad (2)$$

where $F(U)$ is the Rayleigh PDF (probability distribution function), U is the investigated wind speed, and \bar{U} is the mean wind speed for the selected geographical location.

After determining the distribution function, the probable cycle count in a design lifespan could be calculated. $F(U)$ is the probability of a gust of specified strength (or less) happening at a specific instant, and $[1 - F(U)]$ is the probability of a gust having a specified strength or more happening at a particular instant.

Thus, $[1 - F(U)] \times \text{Lifespan} =$ the probable time of exposure to wind of specific speed or greater

For a design lifespan of 50 years, a design wind speed of 120 mph (193 kmh), and an average annual wind speed between 13 mph (21 kmh) and 14 mph (22.5 kmh), the probable number of cycles likely to occur at a wind speed equal to or greater than the selected wind speed can be found by multiplying the calculated exposure duration in seconds by the anticipated vibration frequency. If it is supposed that one full cycle takes place for every exposure second (1 Hz), the expected cycle counts will be equal to the likely seconds of exposure over the chosen design lifespan. As such, the number of reverse-cyclic loadings estimated by the Rayleigh distribution at or above a variety of chosen wind speeds is presented in Table 3.

Table 3. Rayleigh exposure probability at or above specific wind speeds used for testing.

Percentage of the Design Wind Speed [%]	Given Wind Speed [mph]	Probability $1 - F(U)$ [%]	Probable Number of Cycles [#]
10	12	52.72973%	831,442,389
20	24	7.73076%	121,898,627
30	36	0.31514%	4,969,087
40	48	0.00357%	56,320
45	54	0.00024%	3710
50	60	0.00001%	177
60	72	0.00000%	0.2
70	84	0.00000%	0.0
80	96	0.00000%	0.0
90	108	0.00000%	0.0
100	120	0.00000%	0.0

Note: 1 mph = 1.6 kmh.

It should be noted that the Rayleigh distribution is not bound to the design wind speed, as the occurrence probability for a specified wind speed does not vary with a rise in design value. Rather, the distribution is highly dependent on the mean wind speed for any particular area.

4.6. Test Setup

The test setup was designed to test the panels in a vertical position. Lateral load was exerted on the panels by two hydraulic cylinders. The tested panels were configured for testing, as demonstrated in Figures 3 and 4. Two steel columns were provided at the left and right edges of panel. These columns supported an upper steel beam, placed to maintain the panel support condition at the top. Also, the columns supported four cantilevered steel stands with two steel loading beams that spanned the width of the frame. These loading beams corresponded with the quarter height and three-quarter height of the test specimen, with each loading beam reacting a hydraulic cylinder with integrated load cell. The hydraulic cylinders pushed and pulled on steel loading tubes bolted through the concrete face of the test panels. Steel tubes transmitted load only to the thin precast concrete shell and spanned the width of the test panels in an effort to uniformly distribute the applied load.

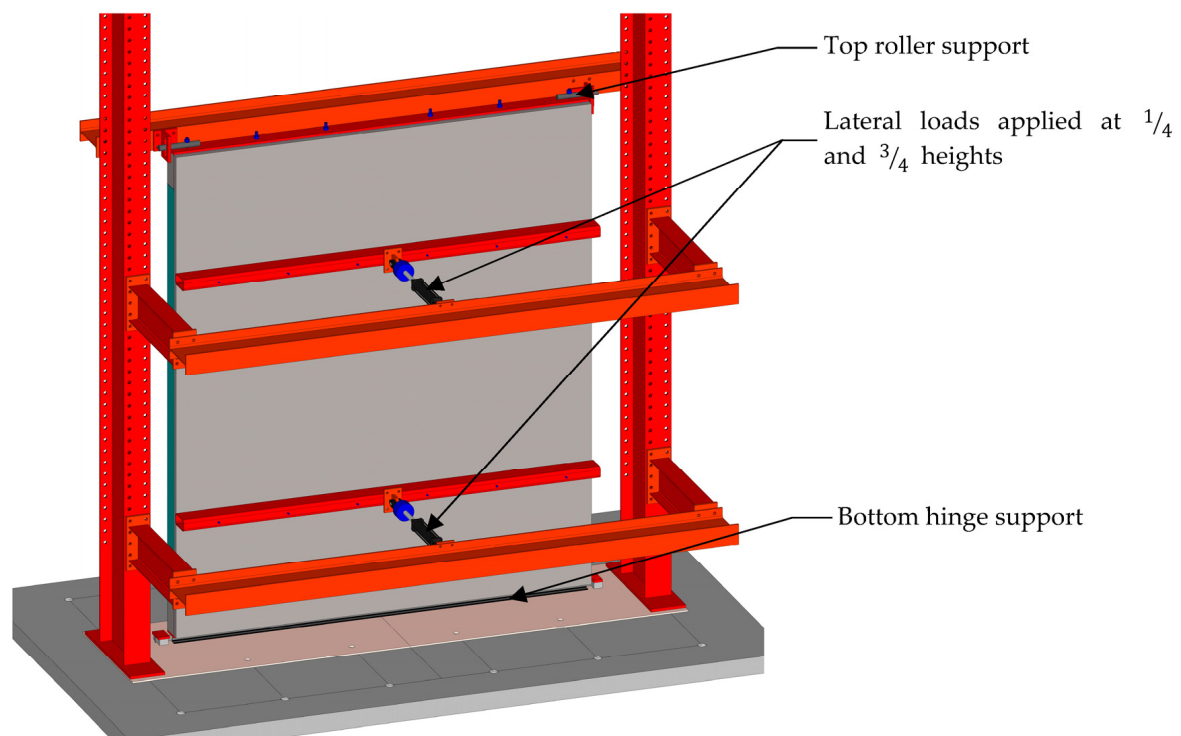


Figure 3. Overview schematic of the test setup.

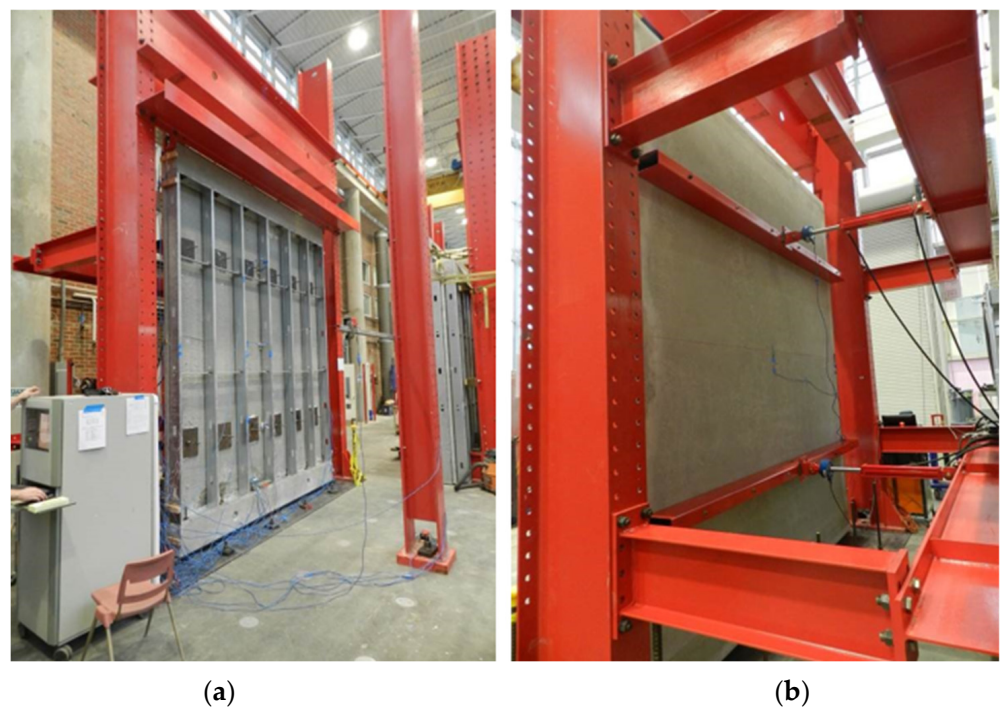


Figure 4. Isometric view of the test setup from (a) back (inner) side and (b) front (outer) side.

The overall setup was built on a strong floor, which enabled a simple support condition for the test panels. The bottom of each panel was supported by a hinge running the full width of the test panel, while the top of the test panel was supported by a slotted pin system, which acted as a bi-directional roller. Lateral motion was restrained at the top of the test panel, but rotations and vertical deflections were allowed. The two hydraulic cylinders were plumbed and controlled to produce matching loads at all times. Lateral load

was applied in accordance with the wind fatigue cycles (pressure and suction) described in the section above.

4.7. Instrumentation

Various instruments were utilized to measure the panels' behaviors by monitoring the loads, deflections, and strains. The instrumentation is listed below:

1. Load cells;
2. String potentiometers (string pots);
3. Linear potentiometers (linear pots);
4. Strain gauges applied to the concrete surface;
5. Strain gauges applied to the steel studs.

A data collection system was utilized to record the data gathered from the instruments. Data were acquired incessantly at a sample rate of 1 Hz throughout static loading and 10 Hz along fatigue loading. Locations of the instruments are indicated in Figure 5. Sign conventions are also provided with instrument locations designated as 'left', 'right', 'back (inner)', and 'front (outer)'. All deflection data provided in the next sections are plotted with respect to the stated sign convention, and they are set to clear the influence of support motion.

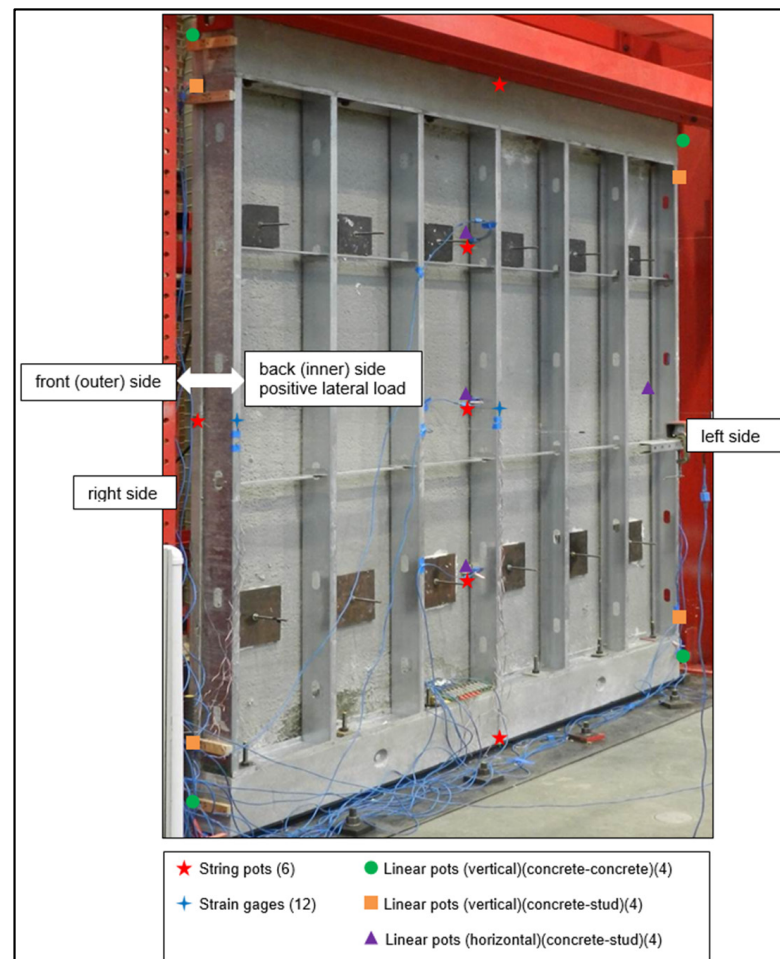


Figure 5. Measurement locations.

4.7.1. Load Cells

A load cell was attached to each hydraulic cylinder. The load cells were utilized to continuously monitor the applied lateral loads.

4.7.2. String Potentiometers

The panel's lateral deflections were monitored throughout the testing with six string potentiometers, as shown in Figure 5. String potentiometers were placed at the mid-width bottom, 1/4 height, mid-height, 3/4 height, and top of the concrete panel. Also, one string potentiometer was located at the right side, mid-height of the concrete panel. Locations of the string potentiometers are demonstrated in Figure 6.



Figure 6. String potentiometer positions.

4.7.3. Linear Potentiometers

In total, twelve linear potentiometers were utilized for the tests, as presented in Figure 5. Four of the linear potentiometers were applied to measure the relative vertical motion between the panel and the concrete beams, as presented in Figure 7a. These potentiometers were placed at the left and right sides of the concrete panel's bottom and top parts, exactly 6 in. (152 mm) from the bottom and the top of the concrete panel.

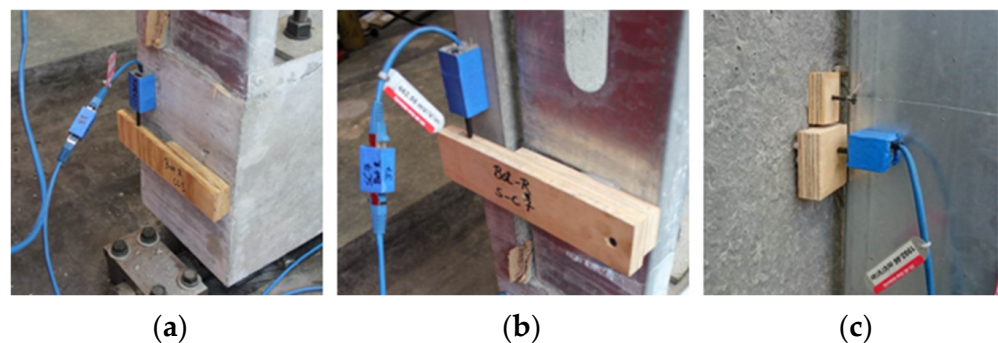


Figure 7. Potentiometers measured (a) relative vertical motion between the concrete panel and the concrete beam, (b) relative vertical motion between the concrete panel and the studs, and (c) relative horizontal motion between the concrete panel and the studs.

Four linear potentiometers were utilized to evaluate the relative vertical motion between the panel and the studs, as demonstrated in Figure 7b. These potentiometers were located at the left and right sides of the bottom and top of the concrete panel, exactly 6 in. (152 mm) from the bottom and top of the steel framing.

Lastly, four potentiometers were utilized to measure the relative horizontal motion between the concrete panel and the studs, as shown in Figure 7c. These potentiometers were mounted mid-width, at the 1/4 height, mid-height, and 3/4 height locations of the concrete panel. In addition, one potentiometer was located mid-height at the left edge of the concrete panel.

4.7.4. Strain Gauges

In order to monitor strains in the thin-shell wall panels, four surface-applied strain gauges for concrete were utilized at the mid-height on the front and back parts of the concrete panel, at the mid-width and on the right edge, as presented in Figure 8.

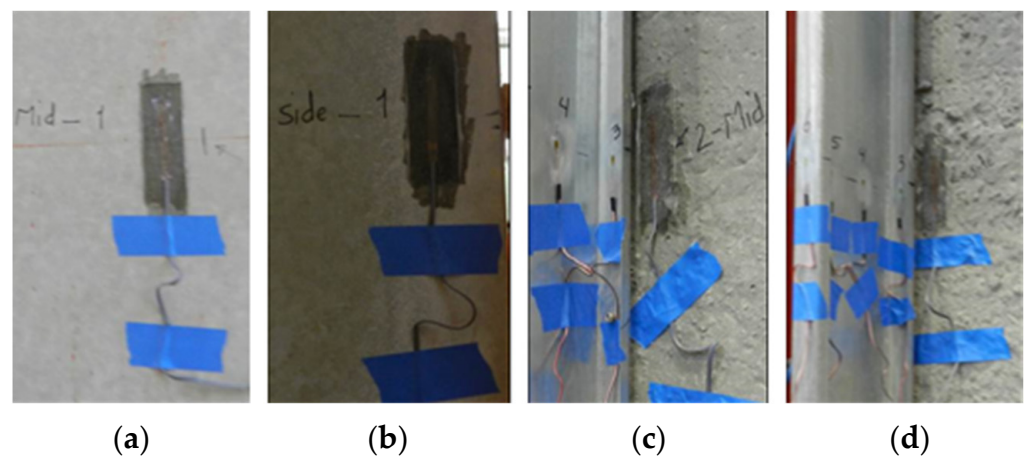


Figure 8. Locations of the strain gauges on concrete: front side, mid-height at (a) mid-width and (b) right edge, and the back side, mid-height at the (c) mid-width and (d) right edge.

Moreover, eight strain gauges for steel studs were used at the mid-height of the back side of the concrete panel, on the steel studs located at mid-width and along the right edge, as shown in Figure 9. For all strain measurements, tension is considered positive.

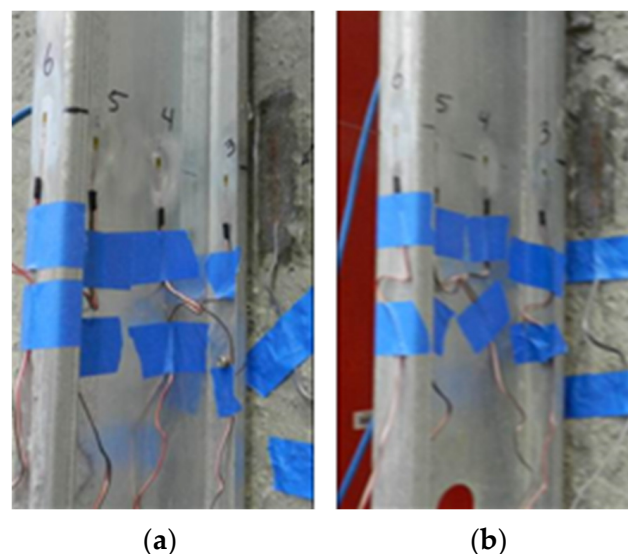


Figure 9. Locations of strain gauges applied on steel studs: back-side, mid-height at the (a) mid-width, and (b) right-side.

5. Test Results and Discussion

Test results from the two thin-shell, non-load-bearing wall panels are examined in the subsequent sections.

5.1. Loading Sequence

The aforementioned loading sequence was followed for the tests. Each fatigue cycle comprised a windward load (positive direction, concrete shell pressed towards steel studs) and a leeward load (negative direction, concrete shell pulled away from steel studs) of the same magnitudes. Cycles were applied in load control at a 5 s per cycle (0.2 Hz) or less loading rate.

5.1.1. Panel NLB-1

The first specimen, Panel NLB-1, was loaded in the prescribed steps up to $90\% \times 60 = 54$ psf (2.59 kPa), which was the maximum measured lateral load prior to failure. This failure level is equivalent to a 9 kips (40 kN) total lateral load. Panel NLB-1's lateral loading corresponds to a 120 mph design wind speed (193 kmh). All load steps followed during the test of the NLB-1 thin-shell panel are summarized in Table 4. The positive/pushing part of each load cycle was finished prior to the negative/pulling portion of each cycle for any given load level.

Table 4. Experimental loading sequence for NLB-1 panel.

Step Number	Applied Lateral Load Steps		
	Load Level [psf]	Load Per Cylinder [kips]	Cycles Completed [#]
1	0	0	0
2	$35\% \times 60 = 21$ psf	1.75	4697
3	$40\% \times 60 = 24$ psf	2	96
4	$45\% \times 60 = 27$ psf	2.25	1
5	$50\% \times 60 = 30$ psf	2.5	1
6	$60\% \times 60 = 36$ psf	3	1
7	$70\% \times 60 = 42$ psf	3.5	1
8	$80\% \times 60 = 48$ psf	4	1
9	$90\% \times 60 = 54$ psf	4.5	Separation of the top concrete beam from the thin outer shell

Note: 1 psf = 0.048 kPa; 1 kips = 4.45 kN.

5.1.2. Panel NLB-2

The second specimen, Panel NLB-2, was loaded up to a maximum measured load of $110\% \times 60 = 66$ psf (3.16 kPa) before failure. This failure is equivalent to 11 kips (49 kN) lateral loading. The NLB-2 panel's lateral loads correspond to 120 mph (193 kmh) design wind speed. All load steps followed during the test of the NLB-2 panel are presented in Table 5. As with NLB-1, the positive segment of each load cycle was completed before the negative.

Table 5. Experimental loading sequence for NLB-2 panel.

Step Number	Applied Lateral Load Steps		
	Load Level [psf]	Load per Cylinder [kips]	Cycles Completed [#]
1	0	0	0
2	$35\% \times 60 = 21$ psf	1.75	4697
3	$40\% \times 60 = 24$ psf	2	96
4	$45\% \times 60 = 27$ psf	2.25	1
5	$50\% \times 60 = 30$ psf	2.5	1
6	$60\% \times 60 = 36$ psf	3	1
7	$70\% \times 60 = 42$ psf	3.5	1
8	$80\% \times 60 = 48$ psf	4	1
9	$90\% \times 60 = 54$ psf	4.5	1
10	$100\% \times 60 = 60$ psf	5	1
11	$110\% \times 60 = 66$ psf	5.5	Separation of the top concrete beam

Note: 1 psf = 0.048 kPa; 1 kips = 4.45 kN.

5.2. Failure Mode

5.2.1. Panel NLB-1

The NLB-1 panel was loaded in balanced cycles up to the $90\% \times 60 = 54$ psf (2.59 kPa) load level, with the panel behaving in a generally elastic manner through the previous load level. No cracks were observed on either face through the $80\% \times 60 = 48$ psf (2.3 kPa) load level. Failure was observed because of the detachment of the top R/C beam block from the concrete shell, with the corresponding rupture of the internal CFRP grid. This separation occurred on the pull stroke of the 54 psf (2.59 kPa) cycle, as shown in Figure 10.

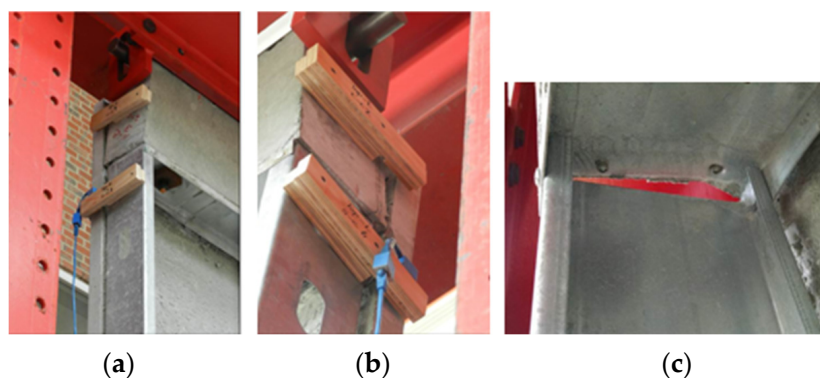


Figure 10. Views of the top of NLB-1 at failure at the right (a) and left (b) ends show separation of the integrated concrete beam, and (c) shows separation of a typical steel stud from the top track.

This specimen had survived the prior push stroke to the same load level with no issue. Panel failure was seen with a sudden decrease in lateral load capacity. Separation between the top steel track and the steel studs was also observed at and beyond failure, as presented in Figure 10c.

Figure 11a presents the separation at failure of the top R/C beam block from the concrete shell at the XPS foam layer, including rotation of the top steel track and separation of the track from the steel studs. The observed failure mode did not involve the rivets that provide interlock between the steel stud flanges and the concrete panel, as presented in Figure 11b. Figure 11c shows rupture of the CFRP grid at failure. The rivets and associated air gap between the concrete shell and steel stud flanges remained intact after failure.

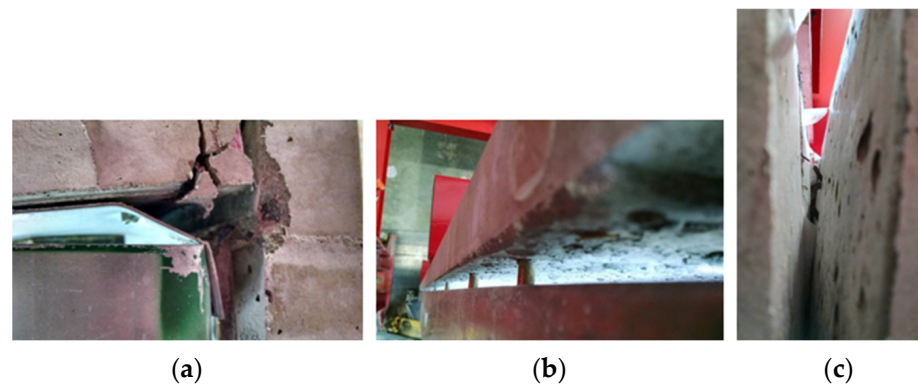


Figure 11. Views of the NLB-1 panel after failure. (a) Rotation of the top integrated concrete beam and connected steel track. (b) A view of the rivets down one stud still connected to the concrete shell after failure. (c) Internal CFRP grid rupture at the top integrated R/C beam.

5.2.2. Panel NLB-2

The NLB-2 panel was loaded in balanced cycles up to the $110\% \times 60 = 66$ psf (3.16 kPa) load level, and this panel also behaved largely elastically up to this load level. No cracks were observed on either face of the concrete shell through the $100\% \times 60$ psf (2.9 kPa) load level. As with the first specimen, the failure happened because of the detachment of the top R/C beam block from the concrete shell at the XPS insulation layer and was accompanied by partial rupture of the internal CFRP grid. This separation occurred for NLB-2 on the pull stroke of the $110\% \times 60 = 66$ psf (3.16 kPa) load cycle, as shown in Figure 12. The specimen survived the prior push stroke to the same load level with no visible damage. Failure of the panel corresponded with a sudden decrease in lateral load-bearing potential. Failure also included separation between the top steel track and the steel studs, as presented in Figure 12c. As the steel track was attached to the bottom part of the integrated concrete beam, it was pried away from the studs as the integrated beam rotated away from the concrete face shell at failure. The CFRP grid at failure is demonstrated in Figure 13.

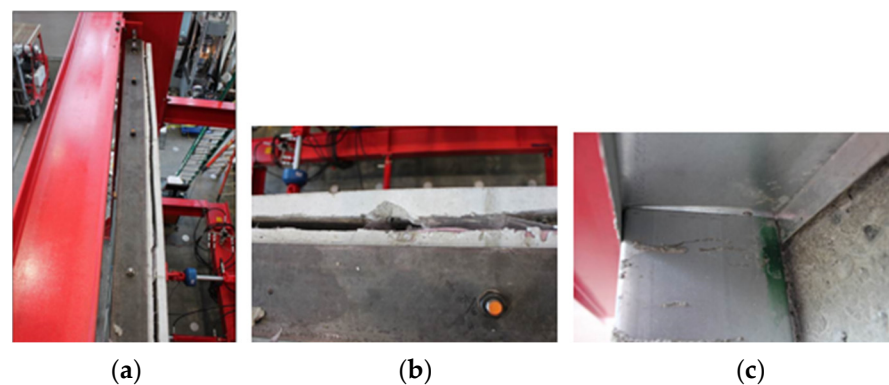


Figure 12. Views of NLB-2 after failure, including (a) looking down from the top, (b) close view of outer shell separation from integrated concrete beam, and (c) top track separating from steel stud.

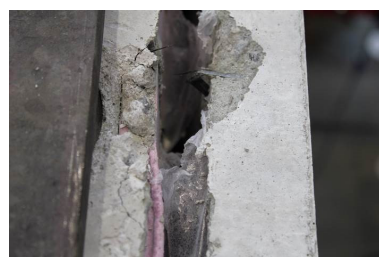


Figure 13. CFRP grid rupture at failure at the top of panel NLB-2.

5.3. Lateral Load Distribution during Testing

Tests of both panels NLB-1 and NLB-2 were conducted using two hydraulic cylinders to apply equal lateral loads, one cylinder at the panel quarter height and one cylinder at the three-quarter height. Thus, verifying that these applied loads matched as intended at all test stages was critical. Both applied loads in a given test were measured independently during all stages of loading and were confirmed to match within 1% of each other at all test ranges. As such, the results below are expressed in terms of “total applied load”, which is the sum of both loads applied to a panel at any selected point of the test.

5.4. Measured Lateral Deflections

Lateral deflections were measured at selected places, as described previously. The deflections were gauged from a stable column supported independently from the panels and independently from the panel testing frame. Positive deflections are considered as movement from the outside of the panel to the inside of the panel or, if stated otherwise, from the concrete shell towards the steel studs. All lateral deflection data were corrected by the measured top and bottom lateral support deflections, which were small at all stages of loading.

5.4.1. Panel NLB-1

The measured lateral deflections for panel NLB-1, corrected for minor measured support motions, are shown in Figure 14. The total applied lateral load (sum from both hydraulic cylinders) vs. measured deflection responses at the panel’s mid-height are shown at the mid-width and right panel edge in Figure 14a. The measured lateral load-deflection behavior along the panel mid-width is presented for the quarter-height, mid-height, and three-quarter-height locations in Figure 14b. These results indicate a linear load-deflection response through about the $40\% \times 60 = 24$ psf [1.15 kPa] load level. Loading and unloading generally take place along the same path in this range, with no visible signs of significant hysteresis over the nearly 5000 loading cycles conducted in this range. This result is an excellent sign that damage did not accumulate at a significant rate through the early loading cycles.

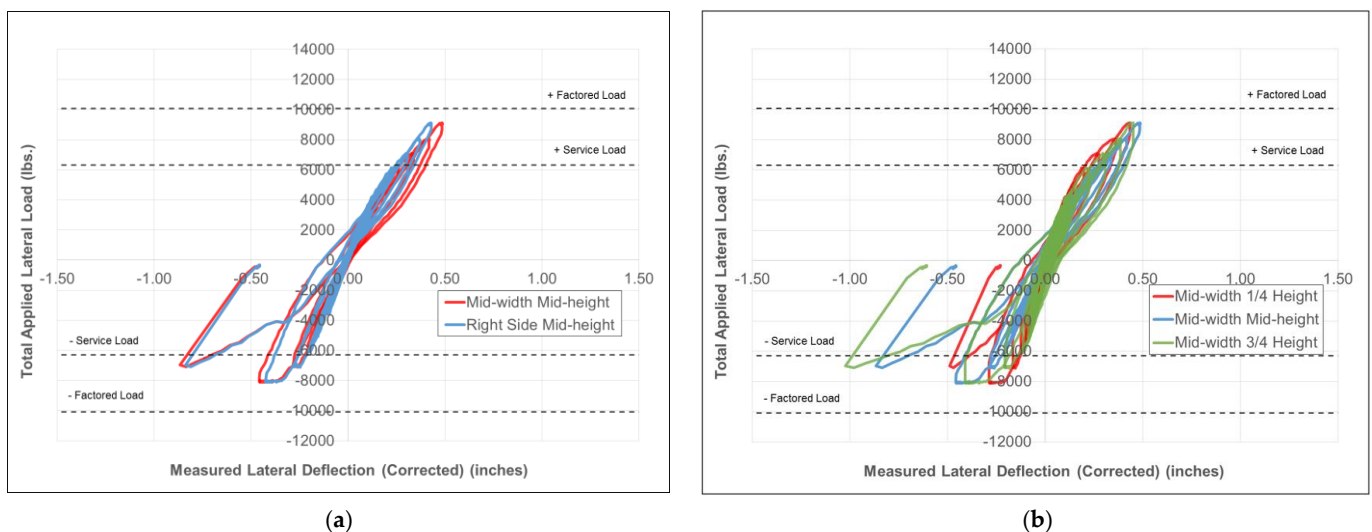


Figure 14. Measured load-deflection response for panel NLB-1 at (a) mid-height locations at the panel mid-width and right edge and (b) mid-width locations at various heights.

At higher levels of load above approximately 40% of the ultimate design level, subtle non-linearity in the load-deflection response develops, with the panel exhibiting a reduced lateral stiffness with increasing lateral load. The ultimate failure is exhibited by significantly increased deflections on the pulling leg of the final loading cycle, as compared to deflections

measured on the prior cycle. Deflections begin to increase more rapidly with increasing load until lateral load-bearing capacity is lost. The result shows that damage accumulated during the prior 80% lateral load cycle and the pushing leg of the 90% loading level was likely sufficient to trigger failure in the final leg of the final cycle. A slight horizontal segment is observed in the load-deflection behavior at the peak of the pulling leg of the 80% \times 60 = 48 psf [2.3 kPa] load cycle. This horizontal behavior indicates increasing deflections under this sustained load, likely due to damage accumulating in the CFRP grid connection at the top of the panel while this connection was in tension. Similar horizontal behavior is not seen at the peak of the positive pushing cycles, likely because the CFRP grid would be in tension during these cycles.

5.4.2. Panel NLB-2

The measured load-deflection behavior for panel NLB-2 is shown in Figure 15, also corrected for minor measured support deflections at the panel's top and bottom. The presented data and behavior are similar to that described above for NLB-1; however, panel NLB-2 exhibited nearly linear load-deflection behavior through higher load levels, roughly corresponding to the service level of 60% \times 60 = 36 psf (1.72 kPa). Beyond the service level, the lateral-load deflection behavior of NLB-2 indicates a decrease in stiffness, with stable behavior observed through the factored level. The localized horizontal segments of the load-deflection behavior observed at certain load level peaks for NLB-1 are not present in the data for NLB-2, indicating that damage to the CFRP connection in NLB-2 developed at higher level loading cycles than it did in NLB-1. At loads beyond the factored level, NLB-2 sustained a pushing cycle to 110% \times 60 = 66 psf (3.16 kPa) with the CFRP connectors in compression but was unable to sustain this load level with the hydraulic cylinders pulling, with the CFRP connectors in tension. Failure of NLB-2 was accompanied by a rapid increase in lateral deflections at constant load with subsequent rapid loss of load-carrying capacity. The load-deflection behavior is consistent with a loss of tension capacity in the CFRP connectors at the panel's top.

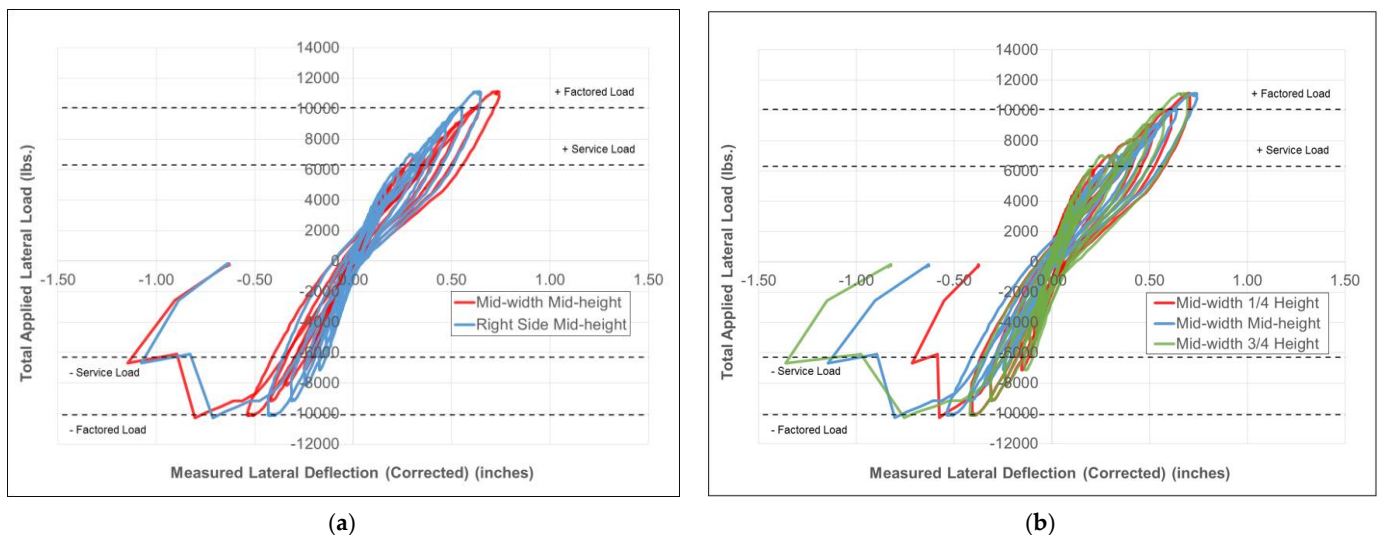


Figure 15. Measured load-deflection response for panel NLB-2 at (a) mid-height locations at the panel's mid-width and right side and (b) mid-width locations at various heights.

5.5. Measured Relative Vertical and Horizontal Displacements

In addition to measuring the lateral deflections of the panels as a whole, measurements were taken of the relative vertical and horizontal displacements at several locations. Four linear potentiometers were used to determine the relative vertical displacement among the concrete panel and the concrete beams. Four linear potentiometers were utilized to measure the relative vertical displacement between the concrete panel and the studs. Details about

the locations of these instruments were described earlier. The sign convention for these instruments considered an upward motion of the concrete shell relative to the steel stud or concrete beam to be positive vertical motion and an opening of the gap between the shell and steel stud and positive horizontal motion. As such, positive vertical motions at the top of the panel would generally be expected at the top of the panel with positive applied lateral loads, as would positive horizontal motions. Negative vertical motions at the bottom of the panel would generally be expected with positive applied lateral loads.

5.5.1. Panel NLB-1

Relative vertical displacement among the concrete shell and the top and bottom concrete beams for panel NLB-1 is shown in Figure 16a. The data indicate that the bottom concrete beam moved upwards relative to the concrete shell with a positive lateral load (pushing on the shell). In the negative loading case, with loading hardware pulling on the shell, the relative vertical displacements of the concrete beams are in the opposite direction, as expected. Relative movement of the bottom beam was small throughout the loading range; however, movement of the top beam relative to the concrete shell became significant on the pulling legs (negative applied lateral load) of each cycle. The relative movement of the top concrete beam on the positive leg of each loading cycle was small, even at high load levels. This result confirms the idea that the CFRP connection between the beam and shell was durable with the joint in compression (when the CFRP was lightly stressed) but was accumulating damage on the pulling legs of higher-level load cycles when the CFRP was in tension. Significant slip between the top concrete beam and the concrete shell is observed on the pulling leg of the 80% loading cycle and then on the pulling leg of the subsequent 90% loading cycle when the panel fails.

Relative vertical motions between concrete shell and steel studs are plotted in Figure 16b. These data indicate the deflection trends expected, with the panel concrete shell moving upwards relative to the steel stud at the panel's top under positive load and downwards relative to the steel stud at the bottom of the panel under positive load. The trend is reversed under negative load. The data indicate a stable connection between steel studs and concrete with regard to slip in the vertical direction; however, some damage is observed to accumulate at this connection at higher-level load cycles, based on the observed non-linearity. Such damage indicates a behavior between a steel stud and a concrete shell that is not fully composite.

Relative horizontal displacements between the concrete shell and the steel studs are presented in Figure 16c. It can be observed from the figure that the gap between the steel stud and concrete shell closed partially under positive lateral loading and opened slightly under negative lateral loading, as expected. Surprising, however, was the fact that the magnitude of gap closing exceeded the magnitude of gap opening, indicating that the rivets connecting steel studs and concrete shell slipped into the concrete shell under compression more than they pulled out of the concrete shell under tension. This result is confirmed by visual observations and video taken during testing and indicates localized concrete crushing under embedded heads of the rivets, or possibly air bubbles or other poor consolidation in these very localized areas. Despite this, measured motion in compression of up to 0.1 in. (2.5 mm), the horizontal load-deflection relationship remained stable and did not seem to influence panel capacity. The rivet-to-concrete connection, however, did appear to accumulate damage during cycling, as indicated by the hysteresis observed in the load-deflection behavior. This damage likely reduced the composite action of the panel with increasing load and possibly increased the level of demand placed on the upper beam-to-shell connection. Relative displacements between the concrete shell and integrated beam are demonstrated in Figure 17.

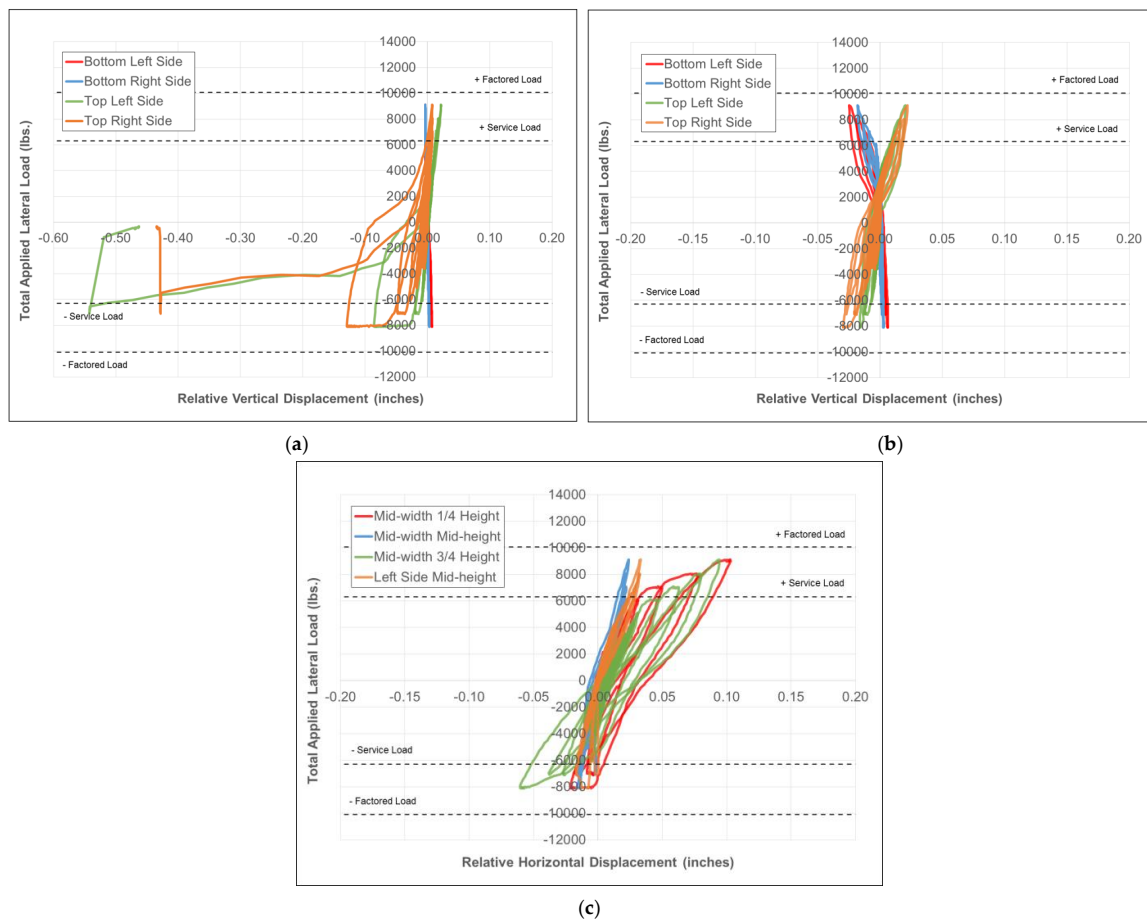


Figure 16. Total applied lateral load vs. measured relative displacement for NLB-1 is plotted: (a) vertically between the concrete shell and concrete beams; (b) vertically between the concrete shell and the steel studs; and (c) horizontally between the concrete shell and steel studs.



Figure 17. Relative displacement of integrated concrete beam to shell at failure.

5.5.2. Panel NLB-2

Relative vertical displacements for Panel NLB-2 between the concrete beam and the shell are shown in Figure 18a. The general behavior matches that observed for Panel NLB-1, with the exception of the “Top Right Side” instrument, which appears to have slipped during testing. Nonetheless, the data between beams and shell show far greater relative

motion when the beam–shell connection is in tension as opposed to compression, and the top beam shows far more motion in general than the bottom beam. This finding also confirms the limitation in CFRP connection strength described above.

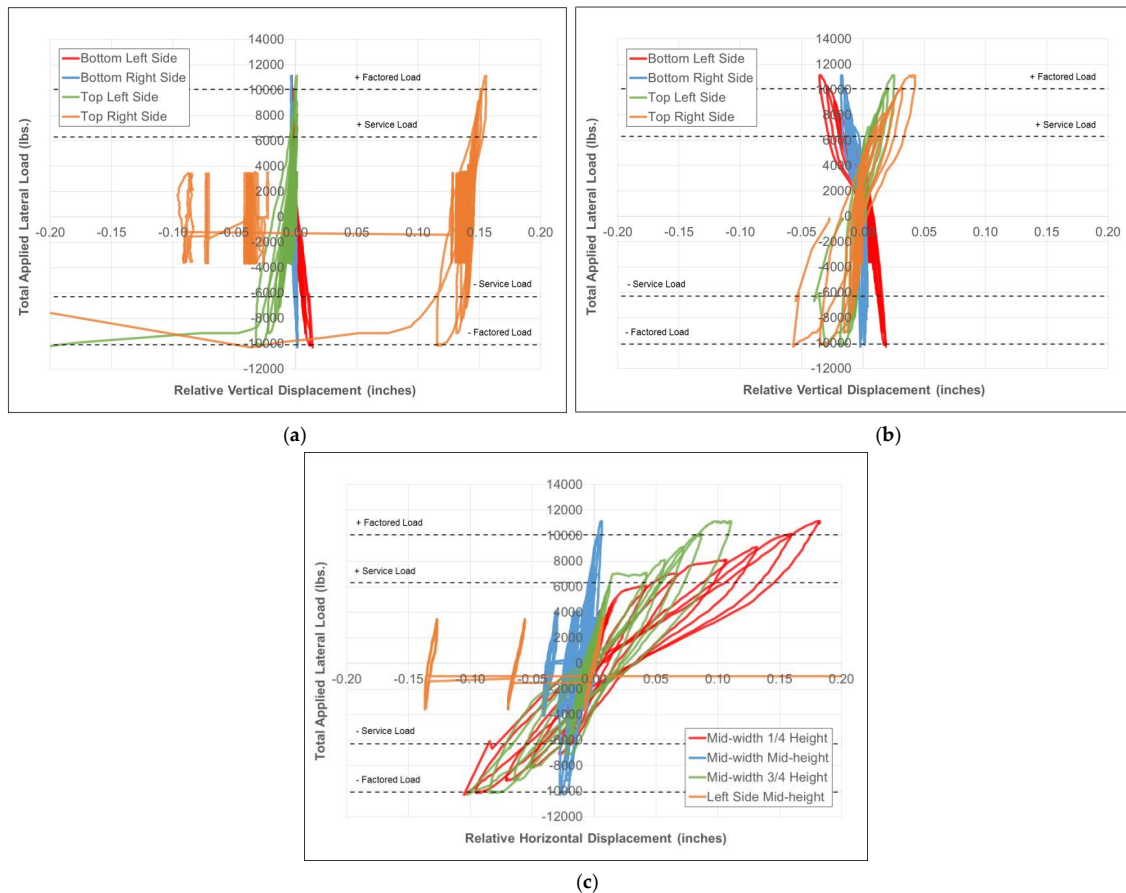


Figure 18. Total applied lateral load vs. measured relative displacement for NLB-2 are plotted: (a) vertically between the concrete shell and concrete beams (Top Right instrument slipped during testing); (b) vertically between the concrete shell and the steel studs; and (c) horizontally between the concrete shell and steel studs (Left Side Mid-height instrument slipped and should be considered unreliable).

Relative vertical deflections between stud and shell are shown in Figure 18b and also generally match the trends observed for panel NLB-1. Steel stud to concrete shell motion is small and stable; however, non-linearity and hysteresis in the load-deflection behavior indicate some accumulating damage, which likely corresponds with decreasing composite action with increasing applied lateral load.

Relative horizontal deflections between the concrete shell and steel studs are again surprising, indicating substantial slip between the concrete and the rivets in compression more so than in tension, as shown in Figure 18c. Again, this observation was confirmed with observations and video taken during testing. Note while reviewing Figure 18c that the “Left Side Mid-height” instrument likely slipped during loading and should be deemed unreliable. The remaining instruments, however, clearly show a relatively large closing of the gap between the concrete shell and steel stud under applied positive load, indicating that the rivets are locally crushing the concrete of the face shell in compression or that this concrete locally was not well consolidated very locally under the heads of the embedded rivets.

5.6. Measured Strains

Four strain gauges were utilized to measure the flexural strains at the mid-height of the front and back faces of the concrete shell at the panel mid-width and at the right side. Also, eight strain gauges were utilized at the mid-height of the back side of the concrete panel on the steel studs at mid-width and at the right side, as described previously. It should be noted that for all strain measurements, tension strain is considered positive. Mid-width and right-side gauge locations are identified as 1, 2, 3, 4, 5, and 6, corresponding to the strain gauges located at:

1. Outer face of concrete shell on the concrete;
2. The inner face of the concrete shell (steel stud side) on the concrete;
3. On the flange of steel stud closest to the concrete;
4. On the web of steel studs closest to the concrete
5. On the web of steel studs farthest from the concrete
6. On the flange of steel stud farthest from the concrete.

5.6.1. Panel NLB-1 Strains

The total applied lateral load vs. measured strain behavior for Panel NLB-1 is plotted in Figure 19a. The measured load-strain behavior of any given gauge was generally linear throughout the loading range, with strain levels remaining below the yield point for steel and below the compression crushing strain for concrete. This result indicates that the fundamental concrete and steel materials were not stressed beyond their limits in flexure and that global flexural behaviors did not govern panel performance. This result confirms the criticality of the connections between integrated beams and the concrete shell and between steel studs and the concrete shell. Behaviors between the mid-width location and the right-side location were generally matching, indicating effective load distribution from the experimental test setup.

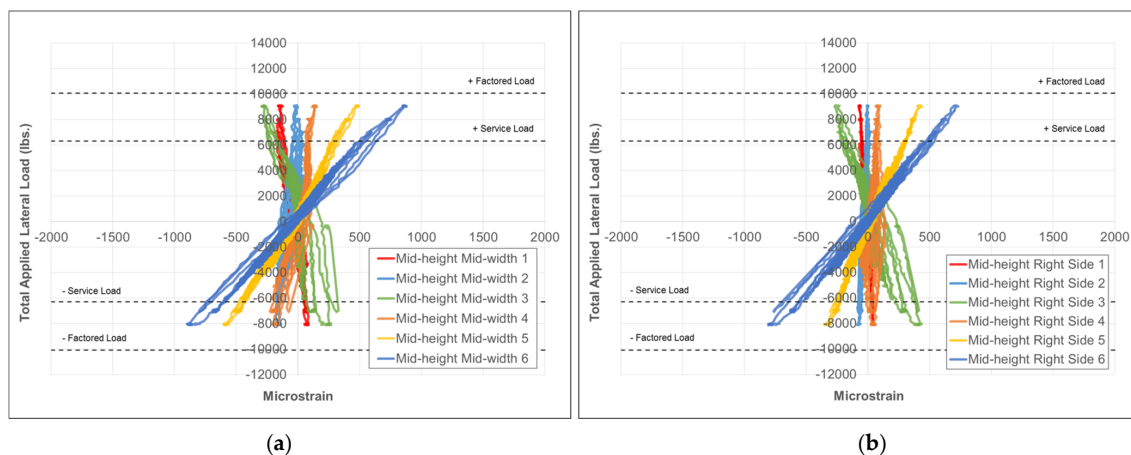


Figure 19. Total applied lateral load vs. measured strains at mid-height for Panel NLB-1 at the (a) mid-width and (b) right side.

The most important finding from the measured strain data is that Panel NLB-1 behaved in a largely non-composite manner, indicating that steel studs and the concrete shell were each bending about a separate neutral axis. Stated otherwise, plane sections did not remain plane through the entirety of the panel cross-section. Examining the sequence of strain gauge measurements from compression to tension at the peak positive applied load indicates that Gauge 3 is the most highly compressed, followed by Gauge 1 and then Gauge 2. Gauge 4 is then slightly in tension, followed by Gauge 5, and then Gauge 6 at the highest level of tension. Stated simply, there is more compression strain in the steel stud flange than in the concrete shell when positive lateral load is applied. This indicates that

slip must occur at the rivets connecting steel studs and concrete shell, and thus, the steel studs can bend about one neutral axis while the concrete shell bends about another.

Strain profiles generated from these data (see Figure 20) confirm this finding. The steel stud strains from Gauges 3, 4, 5, and 6 always fall along a single straight line when plotted as a function of their position, indicating plane sections remained plane within the steel stud. The steel stud strain profiles also always range from tension to compression, indicating a neutral axis falls within the stud itself. Concrete strains are very low and also often range from compression to tension (with one extreme sometimes lying very close to zero), which indicates a second neutral axis is within the concrete shell or very close to one surface of the concrete shell, depending on the loading level and cycle direction.

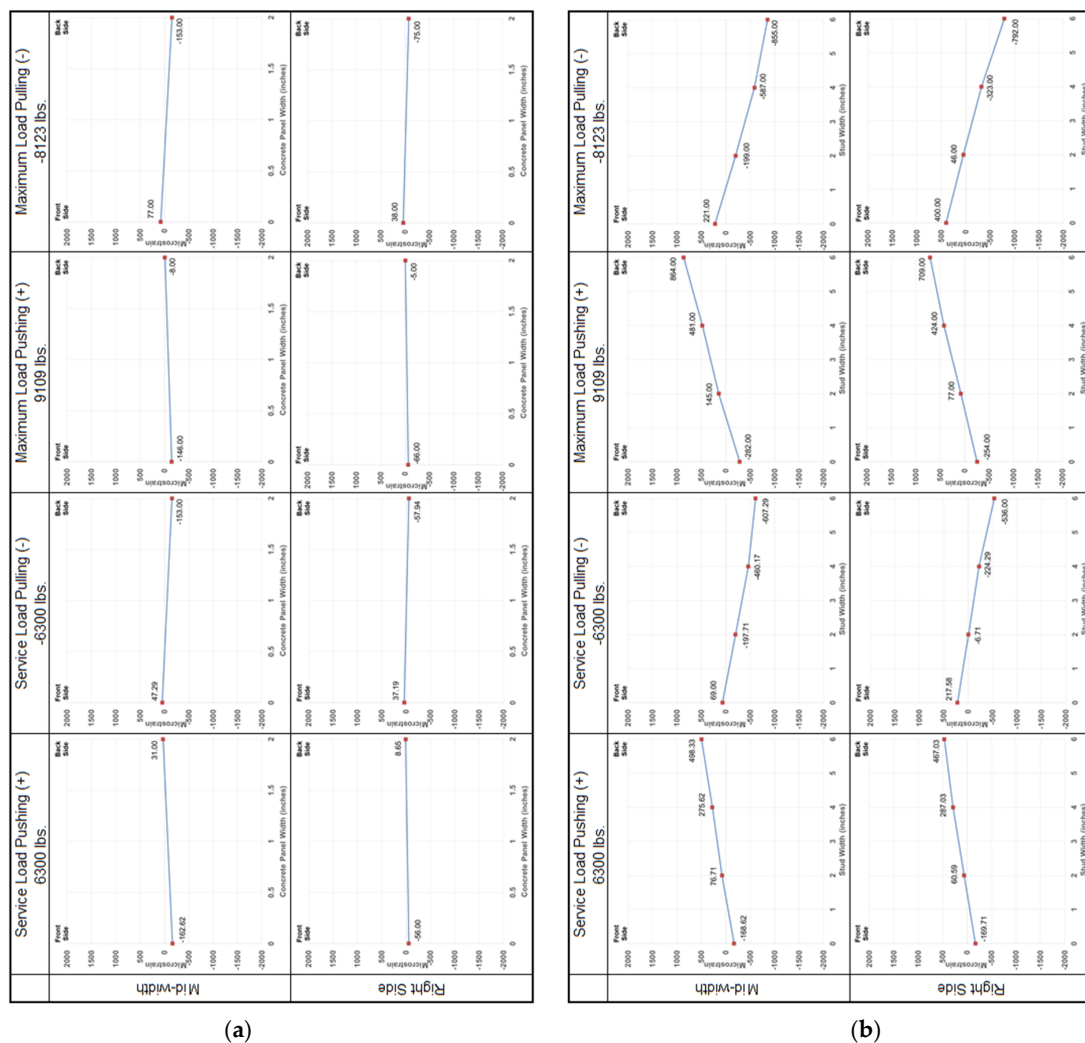


Figure 20. NLB-1 concrete (a) and steel (b) strain profiles at service and maximum load.

5.6.2. Panel NLB-2 Strains

The measured load-strain behavior for panel NLB-2 was similar to that observed for NLB-1, as shown in Figure 21. In reviewing data from the mid-width location in Figure 21a, note that Gauge 2 appears to be debonding and should be considered unreliable. Nonetheless, data from the mid-width location and right edge location are consistent and indicate that compression strains in the steel stud exceed compression strains in the concrete under positive loading, confirming highly non-composite behavior. Strain profiles in Figure 22 for panel NLB-2 confirm the conclusion of largely non-composite performance.

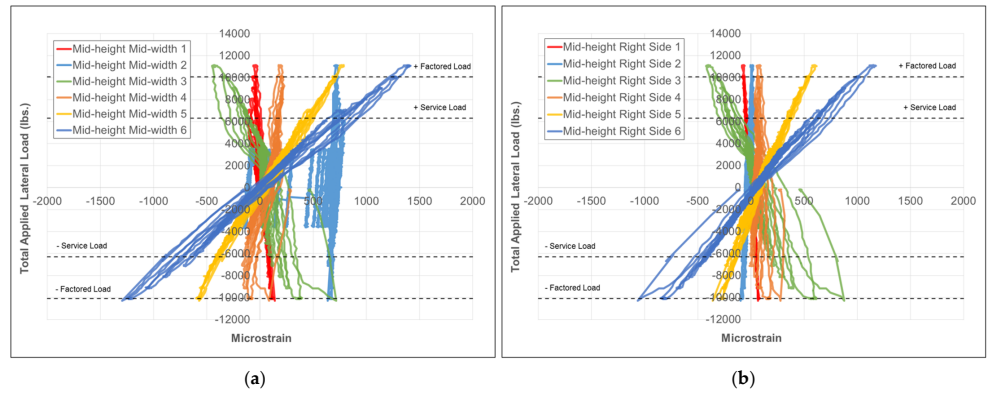


Figure 21. Total applied lateral load vs. measured strains at mid-height for Panel NLB-2 at the (a) mid-width and (b) right side.

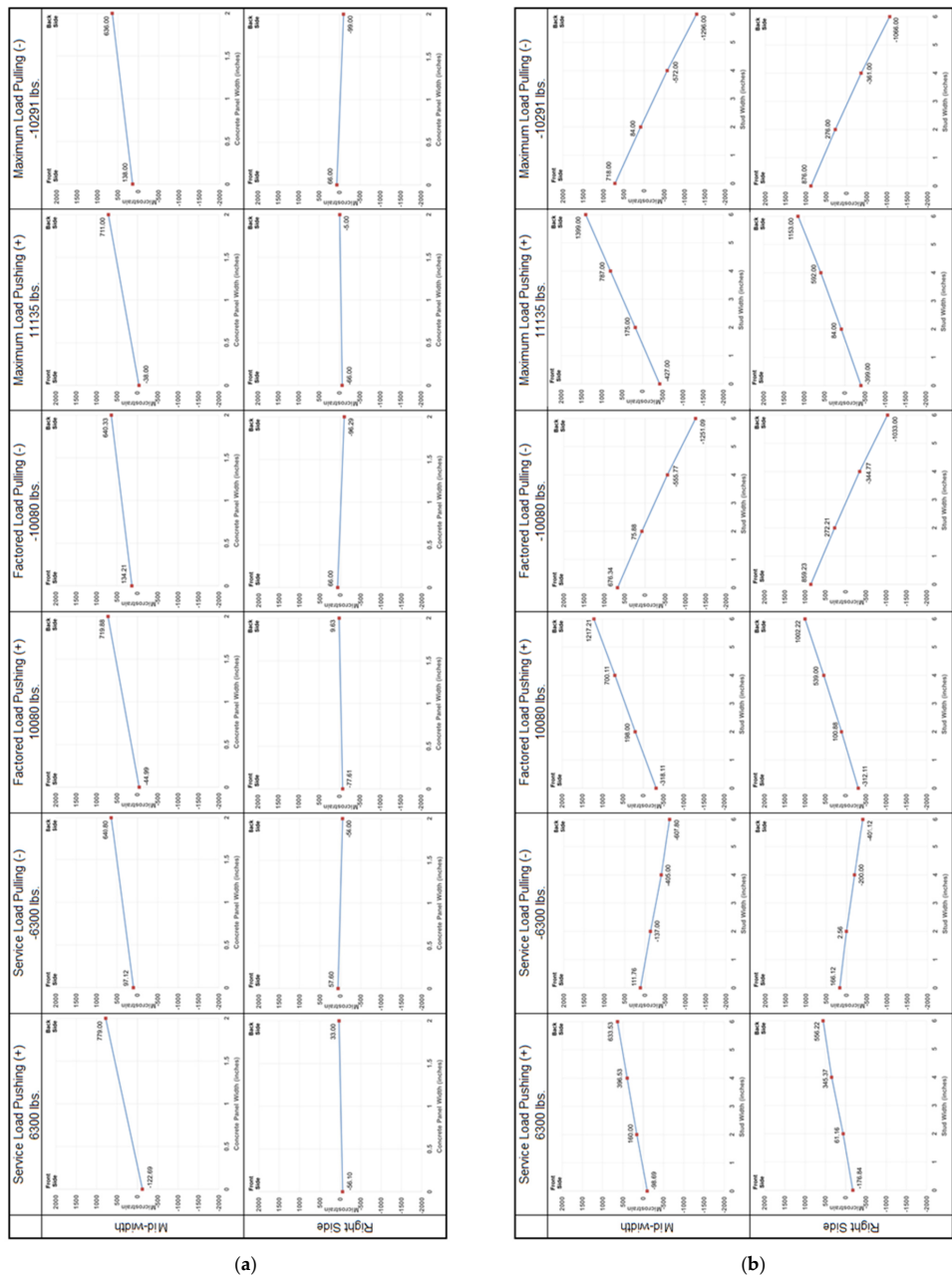


Figure 22. NLB-2 concrete (a) and steel (b) strain profiles at service and maximum load.

6. Conclusions

This paper detailed the tests of two precast concrete non-load-bearing stud–concrete wall panels. The panels consisted of a 12 ft. × 14 ft. (3.7 m × 4.3 m) outer shell of concrete having a thickness of 2 in. (51 mm) and an 11.96 ft. × 12 ft. (3.7 m × 3.7 m) steel stud frame of 6 in. (152 mm) depth. The unique design used a series of rivets to connect the steel studs to the concrete shell along the length of each stud and a CFRP grid to connect two integrated reinforced concrete beams, one at the top and one at the bottom, to the shell through a sheet of rigid foam insulation. The panels were designed to resist lateral wind loads in the pressure or suction directions and were tested under simulated uniform lateral pressure with reverse-cyclic loading to measure the behavior of the panels under this condition. Loads and cycles were configured to mimic a 50-year design life.

Panel NLB-1 failed at a load level of 90% of the ultimate design value. Panel NLB-2 reached a maximum measured load level of 110% of the design value. The capacity of both panels was controlled by the tension strength of the CFRP grid connection at the panel top. This grid connection slipped and ruptured at failure when the connection was placed in tension. The following conclusions are drawn from this testing program:

- The unique design enabled lightweight panels with a thermally isolated concrete shell, separated from the steel stud structure by a continuous air and insulation gap;
- The panels behaved well at their service levels, exhibiting nearly elastic behavior over nearly 5000 cycles of reverse-cyclic lateral loading;
- Panel NLB-1 did not reach its intended ultimate design level, indicating that the top connection between the integrated concrete beam and concrete face shell was insufficient. It is recommended that this connection be strengthened by adding more CFRP grids at a closer spacing or by using a stronger CFRP grid;
- Panel NLB-2 reached and exceeded its intended ultimate design level, indicating that the design was sufficient for this specimen. However, the designs of NLB-1 and NLB-2 were identical, indicating some variability in the manufacturing process influenced the ultimate strength. Improving the connection strength between integrated concrete beams and the concrete shell should improve the average strength of the panels. A final design should achieve the ultimate design level in all tests;
- The rivet connections between steel studs and concrete shell were effective but did allow slip between stud and concrete in the vertical and lateral directions. This slip prevented composite behavior from developing, meaning that the steel studs and the concrete shell were bending about separate neutral axes in flexure. A more efficient design might increase the strength of the connection between steel studs and concrete shell (by reducing rivet spacing) to achieve composite performance in bending. Modifying the rivets to improve the bond between rivets and concrete might also help in this regard.

Author Contributions: Conceptualization, T.S.Y. and G.L.; methodology, T.S.Y. and G.L.; validation, T.S.Y.; formal analysis, T.S.Y.; investigation, T.S.Y. and G.L.; resources, T.S.Y. and G.L.; data curation, T.S.Y.; writing—original draft preparation, T.S.Y.; writing—review and editing, T.S.Y. and G.L.; visualization, T.S.Y.; supervision, G.L.; project administration, G.L.; funding acquisition, G.L. All authors have read and agreed to the published version of the manuscript.

Funding: Metromont Corporation of Greenville, SC, USA, funded the laboratory tests used in this research. Analysis of the data and drafting of this manuscript were not funded.

Data Availability Statement: Data are available upon request at the discretion of the sponsor.

Acknowledgments: The authors would like to express their gratitude to Metromont Corporation for funding the experiments and for fabricating and transporting the test specimens. The authors also would like to thank Sami Rizkalla for his guidance through the experimental program. Furthermore, the authors would like to extend their deepest thanks to the staff of the Constructed Facilities Laboratory at North Carolina State University for their continuous support during the tests.

Conflicts of Interest: The authors declare no conflict of interest.

References

1. Rubio, E.; Rubio, E.J.; Lucier, G.; Moscow, B.; Rizkalla, S.H. Ceramic Precast Composite Panels: High Performance Structural and Architectural Building Enclosures. Facade Techtonics World Congress Proceedings, Volume 1. 2018. Available online: <https://www.facadetechtonics.org/papers/ceramic-precast-composite-panels> (accessed on 20 October 2023).
2. Hofheins, C.L.; Reaveley, L.D.; Pantelides, C.P. Behavior of welded plate connections in precast concrete panels under simulated seismic loads. *PCI J.* **2002**, *47*, 122–133. [[CrossRef](#)]
3. Pessiki, S.; Mlynarczyk, A. Experimental evaluation of the composite behavior of precast concrete sandwich wall panels. *PCI J.* **2003**, *48*, 54–71. [[CrossRef](#)]
4. Choi, I.; Kim, J.; You, Y.-C. Effect of cyclic loading on composite behavior of insulated concrete sandwich wall panels with GFRP shear connectors. *Compos. Part B* **2016**, *96*, 7–19. [[CrossRef](#)]
5. Teixeira, N.; Fam, A. Fatigue behavior of partially composite insulated concrete sandwich walls. *ACI Struct. J.* **2017**, *114*, 125–136. [[CrossRef](#)]
6. Sharafi, P.; Mortazavi, M.; Usefi, N.; Kildashti, K.; Ronagh, H.; Samali, B. Lateral force resisting systems in lightweight steel frames: Recent research advances. *Thin-Walled Struct.* **2018**, *130*, 231–253. [[CrossRef](#)]
7. Tafti, M.R.J.; Behnamfar, F. Investigating the effect of the number of end-panel studs on the seismic properties of cold-formed light-steel shear-panel braces. *Arch. Civ. Eng.* **2013**, *2*, 197–214. [[CrossRef](#)]
8. Iuorio, O.; Macillo, V.; Terracciano, M.T.; Pali, T.; Fiorino, L.; Landolfo, R. Seismic response of CFS strap-braced stud walls: Experimental investigation. *Thin-Walled Struct.* **2014**, *85*, 466–480. [[CrossRef](#)]
9. Accorti, M.; Baldassino, N.; Zandonini, R.; Scavazza, F.; Rogers, C.A. Response of CFS sheathed shear walls. *Structures* **2016**, *7*, 100–112. [[CrossRef](#)]
10. Liu, B.; Hao, J.-P.; Zhong, W.-H.; Wang, H. Performance of cold-formed-steel-framed shear walls sprayed with lightweight mortar under reversed cyclic loading. *Thin-Walled Struct.* **2016**, *98*, 312–331. [[CrossRef](#)]
11. Xu, Z.; Chen, Z.; Yang, S. Seismic behavior of cold-formed steel high-strength foamed concrete shear walls with straw boards. *Thin-Walled Struct.* **2018**, *124*, 350–365. [[CrossRef](#)]
12. Lee, D.-Y.; Cho, B.-H.; Jung, D.-I.; Lee, J.-S.; Lee, K.-W. Experimental study on the cyclic behavior of integrated panels for cold-formed steel shear wall system. *Appl. Sci.* **2020**, *10*, 1649. [[CrossRef](#)]
13. Zhang, X.; Zhang, E.; Zhang, Y. Study on shear performance of cold-formed thin-walled steel walls sheathed by paper straw board. *Eng. Struct.* **2021**, *245*, 112873. [[CrossRef](#)]
14. Belal, M.F.; Serror, M.H.; Mourad, S.H.; El Saadawy, M.M. Seismic behavior of light-gauge cold-formed steel stud walls under monotonic and cyclic loading. *J. Build. Eng.* **2021**, *43*, 103037. [[CrossRef](#)]
15. Bao, W.; Jiang, J.; Shao, Y.; Liu, Y. Experimental study of the lateral performance of a steel stud wall with a semi-rigid connected frame. *Eng. Struct.* **2019**, *183*, 677–689. [[CrossRef](#)]
16. Branston, A.E.; Chen, C.Y.; Boudreault, F.A.; Rogers, C.A. Testing of light-gauge steel-frame—Wood structural panel shear walls. *Can. J. Civ. Eng.* **2011**, *33*, 561–572. [[CrossRef](#)]
17. Eom, T.-S.; Ha, T.-H.; Cho, B.-H.; Kim, T.-H. Cyclic loading tests on framed stud walls with strap braces and steel sheathing. *ASCE J. Struct. Eng.* **2015**, *141*, 04014173. [[CrossRef](#)]
18. Mpilias, N.; Rajabipour, A.; Rodeghiero, B.; Bazli, M. Lateral load capacity of the common steel stud wall framing braced bays in Australia’s Northern Territory. *Case Stud. Constr. Mater.* **2022**, *17*, e01275. [[CrossRef](#)]
19. Morelli, F.; Caprili, S.; Salvatore, W. Dataset on the cyclic experimental behavior of steel frames with reinforced concrete infill walls. *Data Brief* **2018**, *19*, 2061–2070. [[CrossRef](#)]
20. Pali, T.; Macillo, V.; Terracciano, M.T.; Bucciero, B.; Fiorino, L.; Landolfo, R. In-plane quasi-static cyclic tests of nonstructural lightweight steel drywall partitions for seismic performance evaluation. *Earthq. Eng. Struct. Dyn.* **2018**, *47*, 1566–1588. [[CrossRef](#)]
21. Wang, J.; Wang, W.; Pang, S.; Yu, B. Seismic response investigation and nonlinear numerical analysis of cold-formed thin-walled steel tube truss shear walls. *Int. J. Steel Struct.* **2019**, *19*, 1662–1681. [[CrossRef](#)]
22. Prabha, P.; Palani, G.S.; Lakshmanan, N.; Senthil, R. Behaviour of steel-foam concrete composite panel under in-plane lateral load. *J. Constr. Steel Res.* **2017**, *139*, 437–448. [[CrossRef](#)]
23. Dang, L.; Pang, R.; Liu, Y.; Wang, Y.; Wang, L.; Yang, J. Research on seismic performance of precast steel–concrete composite tube shear walls with horizontal joint. *Eng. Struct.* **2022**, *250*, 113409. [[CrossRef](#)]
24. Hanaor, A. Experimental investigation of composite shear panels under cyclic loading. *J. Constr. Steel Res.* **2005**, *61*, 345–369. [[CrossRef](#)]
25. Bunn, W.G. CFRP Grid/Rigid Foam Shear Transfer Mechanism for Precast, Prestressed Concrete Sandwich Wall Panels. Master’s Thesis, North Carolina State University, Raleigh, NC, USA, 2011.
26. *ASCE/SEI 7-16*; Minimum Design Loads for Buildings and Other Structures. American Society of Civil Engineers: Reston, VA, USA, 2017.
27. Erich, H. *Wind Turbines: Fundamentals, Technologies, Application, Economics*, 2nd ed.; Springer: Berlin/Heidelberg, Germany, 2006; pp. 455–458.

28. Xu, Y.L. Determination of wind-induced fatigue loading on roof cladding. *ASCE J. Eng. Mech.* **1995**, *121*, 956–963. [[CrossRef](#)]
29. Manwell, J.F.; McGowan, J.G.; Rogers, A.L. *Wind Energy Explained: Theory, Design, and Application*, 2nd ed.; John Wiley and Sons: Chichester, UK, 2009; pp. 56–60.

Disclaimer/Publisher’s Note: The statements, opinions and data contained in all publications are solely those of the individual author(s) and contributor(s) and not of MDPI and/or the editor(s). MDPI and/or the editor(s) disclaim responsibility for any injury to people or property resulting from any ideas, methods, instructions or products referred to in the content.